

# Reservoir-based deterministic loading of single-atom tweezer arrays

Lars Pause,<sup>1</sup> Tilman Preuschoff,<sup>1</sup> Dominik Schäffner,<sup>1</sup> Malte Schlosser,<sup>1</sup> and Gerhard Birk<sup>1,2,\*</sup>

<sup>1</sup>Technische Universität Darmstadt, Institut für Angewandte Physik,  
Schlossgartenstraße 7, 64289 Darmstadt, Germany

<sup>2</sup>Helmholtz Forschungssakademie Hessen für FAIR (HFHF),  
Campus Darmstadt, Schlossgartenstraße 2, 64289 Darmstadt, Germany

(Dated: August 3, 2023)

State-of-the-art individual-atom tweezer platforms have relied on loading schemes based on spatially superimposing the tweezer array with a cloud of cold atoms created beforehand. Together with immanent atom loss, this dramatically limits the data rate, as the application sequence must be alternated with the time-consuming phases of magneto-optical trapping and laser cooling. We introduce a modular scheme built on an additional cold-atom reservoir and an array of buffer traps effectively decoupling cold-atom accumulation and single-atom supply from the quantum-register operation. For this purpose, we connect a microlens-based tweezer array to a cloud of laser-cooled atoms held in an auxiliary large-focus dipole trap by utilizing atom transport and buffer traps for dedicated single-atom supply. We demonstrate deterministic loading of a hexagonal target structure with atoms solely originating from the reservoir trap. The results facilitate increased data rates and unlock a path to continuous operation of individual-atom tweezer arrays in quantum science, making use of discrete functional modules, operated in parallel and spatially separated.

Published as doi:10.1103/PhysRevResearch.5.L032009

Quantum devices based on individual atoms trapped in large-scale registers of optical potentials have shown their high potential as platforms for quantum simulation and quantum computation in recent years [1–8]. Based on spatial light modulators, multitone acousto-optic deflectors (AODs), or as in our approach, microlens arrays (MLAs), defect-free structures of neutral atoms have been prepared in one dimension [9–12], two dimensions (2D) [13–26], and three dimensions [27–29]. The scalability of these implementations has been demonstrated up to a few hundred qubits [16, 19, 20, 24, 29], while recent advancements have opened a route to controlling thousands of single-atom quantum systems [29, 30]. Furthermore, utilizing Rydberg interactions, the application of 2-qubit operations as well as the simulation of spin Hamiltonians is possible with neutral-atom quantum systems [10–12, 18–20, 22, 31–33].

One remaining challenge of neutral-atom platforms is to access high data rates. A typical experimental cycle starts by preparing a cold-atom ensemble which is loaded into a 2D configuration of dipole potentials. Utilizing collisional blockade, 60% filling with individual atoms is typical [34]. By implementation of gray molasses or dark-state enhanced loading, filling fractions of up to 90% in a system with 100 trapping sites have been demonstrated [15, 35, 36]. Nevertheless, the intrinsic stochastic component limits the performance. Thus, after the loading process, atom resorting is necessary to achieve defect-free structures [26, 37–40]. Each time a prepared structure develops a defect, resorting has to be repeated, and in the case of insufficient spare atoms, the experimental cycle must be started again with cold-atom preparation.

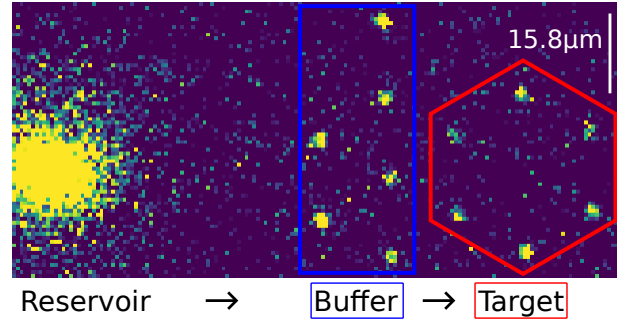


FIG. 1. Single-shot fluorescence image of individual atoms in the hexagonal tweezer array (right) and an atom ensemble in the reservoir dipole trap (left). The blue frame defines the buffer-trap section and the red frame the target structure. The image is taken after four rearrangement sequences and shows a fully filled target structure.

Moreover, the duty cycle is further reduced by qubit readout operations utilizing loss-based detection schemes demanding a new preparation of the target structure after each experimental cycle. This affirms an urgent demand for advanced concepts of individual atom supply.

In the literature, the preparation of registers of individual neutral atoms in large tweezer arrays is based on loading atoms directly from optical molasses being spatially superposed with the whole array. Enhanced loading of atom ensembles has been demonstrated by overlapping a pancake-shaped dipole trap for increased atom density [17]. The spatial overlap of the cold-atom preparation stage and the tweezer array intrinsically limits the duty cycle as magneto-optical trapping (MOT) and molasses phases need to be alternated with single-atom preparation and application sequences. In this letter, we present the concept of separating the sequential steps for defect-

\* Contact for correspondence: apqpub@physik.tu-darmstadt.de; <https://www.iap.tu-darmstadt.de/apq>

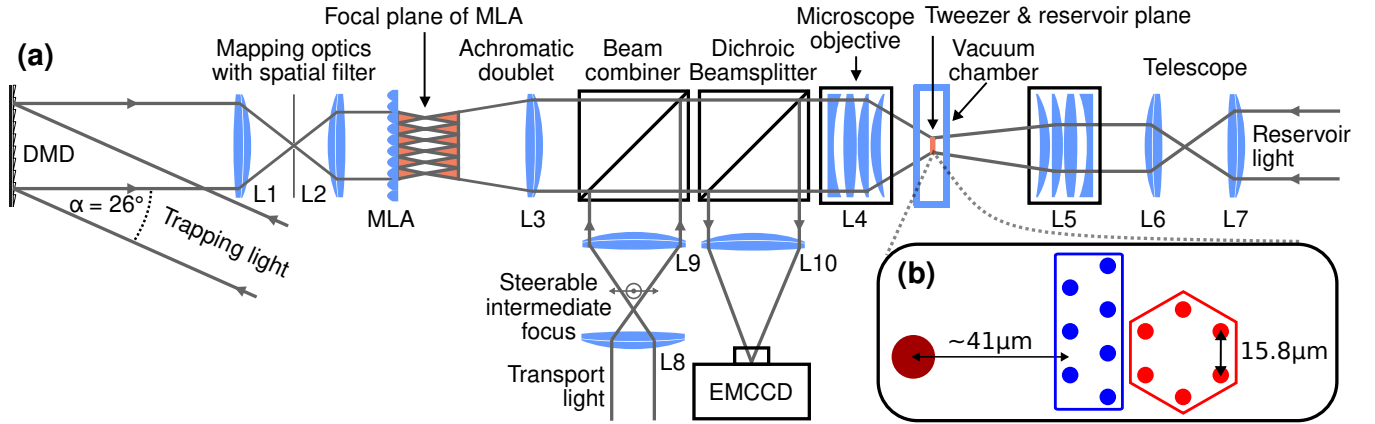


FIG. 2. Reservoir and hexagonal tweezer array setup (not to scale) for deterministic filling of single-atom tweezer arrays. (a) A digital micromirror device (DMD) is illuminated by the trapping light such that the third diffraction order is deflected orthogonally off the DMD surface. Using lenses L1 and L2 the DMD image is mapped onto the microlens array (MLA) whose focal plane is demagnified into the vacuum chamber using the relay optics L3 and L4. With a beam combiner, an acousto-optic deflector (AOD)-based movable laser beam acting as transport tweezers is overlapped with the trapping beam. The reservoir beam, counterpropagating to the tweezer-array laser beam, is focused in the tweezer plane by L5 (equivalent to L4). The waist of this single-beam dipole trap can be adjusted by telescope lenses L6 and L7. The fluorescence light of the trapped atoms is recorded by an electron-multiplying charge-coupled device (EMCCD) camera. Using the DMD, microlenses can be selectively addressed to achieve the trap pattern used in this letter. (b) A schematic of the resulting trap configuration in the tweezer and reservoir plane. The atom reservoir is shown in dark red, and the two tweezer array sections used as buffer and target traps are shown in blue and red, respectively.

free filling of optical tweezers with individual atoms into different functional modules (Fig. 1) designed to be operated sequentially or in parallel. This paves the way for a continuous supply of cold atoms prepared at different times [41] and at different sections of the apparatus [42].

Here, the complete process of deterministic loading of dipole-trap target structures with individual atoms is separated into four modules: (1) preparation of ultracold atoms in a MOT and optical molasses, (2) transfer of a large cloud of ultracold atoms into a large focused-beam dipole trap, i.e., a reservoir trap, (3) extraction of a small ensemble of atoms using movable transport tweezers and application of collisional blockade during transport to a buffer trap section, and finally, (4) deterministic loading of the target structure with individual atoms from the buffer traps, again using transport tweezers. In Fig. 1, a single-shot fluorescence image of trapped atoms exemplifies the overall trap architecture used in this letter: A large focused-beam dipole trap (left) acts as a cold-atom reservoir from which atoms are extracted by the transport tweezers and positioned in the buffer-trap section (blue frame) of a hexagonal array of optical dipole traps. Individual atoms in the buffer traps are then utilized to deterministically fill the target structure consisting of a dipole trap hexagon (red frame).

The schematic of the experimental setup is presented in Fig. 2(a) with the tweezer and reservoir planes shown in Fig. 2(b) in detail. This plane is oriented normal to the central optical axis of the setup. We prepare several  $10^4$  laser-cooled  $^{85}\text{Rb}$  atoms in a custom-made vacuum chamber using six MOT beams and a deceleration

beam, all with a  $1/e^2$  radius of 2.5(1) mm. The atoms are supplied by a rubidium dispenser and slowed using the deceleration beam with an intensity of 6.7(6)  $I_{\text{sat}}$  and a fixed detuning of  $-3.5 \Gamma$  ( $\Gamma = 2\pi \times 6.07 \text{ MHz}$ ) relative to the  $|5S_{1/2}, F = 3\rangle \leftrightarrow |5P_{3/2}, F = 4\rangle$  cooling transition. The MOT consists of four beams with an intensity of 22(2)  $I_{\text{sat}}$  per beam, forming a rectangular cross in a plane oriented at an angle of  $15^\circ$  relative to the tweezer plane and two beams with 30(3)  $I_{\text{sat}}$  per beam, irradiating the atoms at an angle of  $47^\circ$  relative to the tweezer plane. All MOT beams have detuning of  $-2.0 \Gamma$ . The MOT is loaded for 1.8 s, with the deceleration beam being turned off during the final 300 ms. The MOT phase is followed by a molasses phase of typically 40 ms in which the magnetic field is turned off, the cooling laser intensities are reduced to  $\frac{1}{10}$  of the MOT intensities, and the detuning is changed to  $-5.0 \Gamma$ . This results in an atom cloud with a temperature of 22(5)  $\mu\text{K}$ .

A hexagonal array of optical tweezers is created by reimaging the focal plane of a hexagonal MLA with a 750 mm achromatic doublet (L3) and a microscope objective (L4) with a focal length of 37.5(10) mm and a numerical aperture (NA) of 0.25(2) into the vacuum chamber. The fused silica MLA has a pitch of 161.5  $\mu\text{m}$  with a radius of curvature of 2.05 mm for each lenslet. Reimaging creates foci with a pitch of 7.9(1)  $\mu\text{m}$  and a waist of 2.0(2)  $\mu\text{m}$  in the tweezer plane. For selecting a subset of the hexagonal trap pattern and dynamically adjusting the light field illuminating each lenslet, we place a digital micromirror device (DMD) illuminated by a Gaussian laser beam with wavelength of 796.5 nm and  $1/e^2$

radius of  $1.2(1)$  mm in front of the MLA [43]. The DMD is mapped onto the MLA by two achromatic doublets with focal lengths of 50 mm (L1) and 30 mm (L2), respectively. With micromirrors of  $7.64 \times 7.64 \mu\text{m}^2$  size, this results in typically 875 mirrors illuminating each lenslet. For the experiments presented in this letter, we programmed the DMD to double the pitch of the tweezer array to  $15.8(2) \mu\text{m}$  by turning off the illumination of every second lenslet and to generate a configuration of seven buffer traps and a hexagonal target structure of six traps, as shown in Figs. 1 and 2(b). The deepest trap has a trap depth of  $U_{\text{array}}/k_{\text{B}} = 600(200) \mu\text{K}$ . In addition, by adjusting the number of micromirrors illuminating each lenslet, the variation of trap depths within the array is reduced to  $\sim 25\%$ , thus counteracting the intensity variation given by the Gaussian beam profile of the trapping light.

In the modular sequence introduced here, atoms are not loaded directly from the molasses into the trap array, as usual, but are transferred into a large-focus reservoir trap first by superimposing the reservoir potential with the optical molasses for 20 ms. The reservoir trap is created by light at a wavelength of 798.8 nm which is counterpropagating with respect to the trap array beam and focused in the tweezer plane using a second microscope objective (L5). This objective has the same parameters as L4 and is used to create a focus with  $1/e^2$  waist of  $14.6(1) \mu\text{m}$  at a lateral distance of  $41 \mu\text{m}$  from the buffer trap array. The typical trap depth is  $U_{\text{reservoir}}/k_{\text{B}} = 600(200) \mu\text{K}$ . The reservoir occupation is determined by illuminating the atoms with cooling light red-detuned by  $-5.0 \Gamma$  relative to the cooling transition and repumping light red-detuned by  $-0.2 \Gamma$  relative to the  $|5S_{1/2}, F=2\rangle \leftrightarrow |5P_{3/2}, F=3\rangle$  repumping transition. The resulting fluorescence light is recorded for 100 ms with an electron-multiplying charge-coupled device (EMCCD) camera using the objective L4 in combination with a 750 mm achromatic doublet (L10). The imaging time is limited by the NA of the objective L4 as well as the detection efficiency of the camera [16]. The outcome of the resulting stage (2) of the modular sequence gives a reservoir trap typically filled with  $\sim 80$  atoms and no atoms in the microlens-based tweezer array [see Fig. 3 (Frame 1)].

Using movable transport tweezers at a wavelength of 796.5 nm, atoms can be transferred from the reservoir trap to the tweezer array or rearranged within the different segments of the array. The transport tweezers are created using a collimated beam with  $1/e^2$  radius of  $1.5(1)$  mm propagating through a 2D AOD that deflects the beam in both lateral dimensions. The beam is focused by a 60 mm achromatic doublet (L8) to translate the angular deflection into a linear translation. The focus is reimaged into the vacuum chamber by propagating the beam through a 400 mm achromatic doublet (L9) and overlapping it with the trap array beam before passing through the objective L4. This creates transport tweezers with  $1/e^2$  waist of  $2.2(1) \mu\text{m}$  and a scanning range

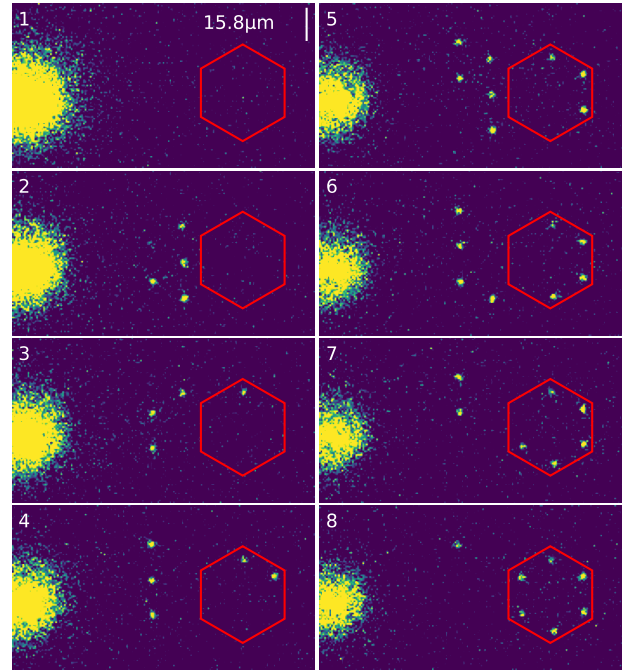


FIG. 3. Series of consecutive fluorescence images of a single experimental realization when loading one atom at a time into a hexagonal target structure (red): Frame 1 shows the filled reservoir trap and the empty tweezer array. In frame 2, the buffer traps have been stochastically loaded with individual atoms from the reservoir. The subsequent frames show the deterministic atom-by-atom loading of the target hexagon.

of  $250 \mu\text{m}$  in both lateral dimensions within the tweezer plane.

We use atoms from the reservoir to load the tweezer array in the next two stages of our modular sequence. For this purpose, we divide the trap array into a region of buffer traps and a target trap section: The buffer traps, marked in blue in Figs. 1 and 2(b), are stochastically loaded from the reservoir and deterministically provide individual atoms for subsequently loading the target structure marked in red. For filling empty buffer traps from the reservoir, we overlap the transport tweezers with the center of the reservoir trap, ramp up the transport tweezer depth to  $U_{\text{T}}/k_{\text{B}} = 800(200) \mu\text{K}$ , and move the trapped atoms with the tweezers to an empty buffer trap position where they are released by ramping down the transport tweezers to zero potential depth. The intensity ramps take  $130 \mu\text{s}$  each, and the movement is performed in  $310 \mu\text{s}$ . During the transport process, the molasses lasers are applied with the same detuning and half the intensity as during the molasses phase for achieving single-atom preparation via light-induced two-body collisions ([15, 34] and references therein). This adds continuous cooling of the atoms, which in general is not necessary for efficient transport [16]. After transport operations to every initially empty buffer trap, the atom configuration is recorded using fluorescence imaging as described above. During atom detection, no two-body

loss occurs in the buffer traps since there is one atom per buffer trap at most. During cooling, transport, and imaging, in the reservoir, two-body atom loss occurs only at a very low rate, as it is inversely proportional to the trapping volume [44]. Due to the large volume of the reservoir trap, the loss rate is three orders of magnitude smaller than for the traps of the tweezer array. After imaging, the atom occupation in the buffer traps is further analyzed. For a sufficiently large number of atoms in the reservoir, a probability of 59.6(4)% for filling the buffer traps with an individual atom is achieved.

In the next functional module of our approach, the individual atoms trapped in the buffer section are used to deterministically fill the empty sites of the target structure. To extract an atom from a buffer trap, we direct the transport tweezers to the respective buffer site, ramp the tweezer depth from zero to  $U_T/k_B = 1600(400)$   $\mu\text{K}$ , move the atom to the intended target site, and release it by ramping the depth to zero again. All intensity ramps and movements have the same timing as for loading of the buffer traps from the reservoir. For this atom rearrangement, we use the shortest-move heuristic sorting algorithm described in Ref. [16]. The transport efficiency between target and buffer traps has been determined to be 75.3(9)%. This sequence is repeated until the target structure is completed or the buffer section is empty. For initiation of a repetitive loading sequence of the target structure, the buffer section is reloaded from the reservoir. From the previous buffer trap occupation and the performed transport moves which empty the buffer traps, we can calculate the resulting atom occupation of the buffer traps. This eliminates the requirement for recording a new image of the atom occupation and thus saves time and avoids atom losses. Using this already available information, reloading of the empty buffer traps is initiated. After this sequence, a fluorescence image such as in Fig. 1 is recorded, updating the complete atom-number status of reservoir, buffer section, and target structure.

To demonstrate composition and maintenance of pre-defined target structures on the underlying grid, we load the six-site hexagon target structure atom by atom, as shown in Fig. 3. Following the initial loading of the reservoir (Frame 1), the buffer traps are loaded from the reservoir (Frame 2), showing that, in this realization in four of the seven buffer traps, individual atoms are available for transfer to the target structure. Next, a sequence of six repetitive cycles (Frames 3 to 8) is started in which the target structure is assembled by transferring one atom per cycle from the buffer to the target section. After each cycle, the buffer traps are reloaded, and the next cycle is started by imaging the present trap occupation. One cycle typically takes 230 ms, of which about 130 ms are necessary for image acquisition and readout. The analysis of the trap occupation and subsequent filling of the target traps typically takes 65 ms, while 35 ms are necessary for buffer refilling. For comparison, the lifetime of the atoms in the tweezer array is 10.0(5) s.

For a typical quantum simulation and computation ap-

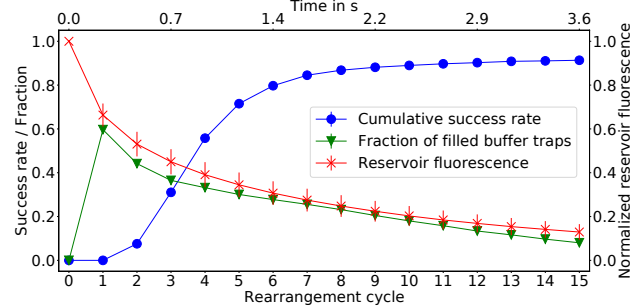


FIG. 4. Quantitative analysis of the reservoir and buffer-trap-based loading of tweezer arrays as a function of the number of rearrangement cycles. Data are based on  $>2500$  experimental repetitions: (Blue) Cumulative success rate of a defect-free target structure of six sites in a hexagonal arrangement. (Red) Normalized reservoir signal corresponding to the atom number inside the reservoir trap. (Green) Average fraction of filled buffer traps available to refill empty target traps. Empty buffer traps are refilled from the reservoir trap during each rearrangement cycle. For the normalized reservoir signal, the uncertainty is given by the standard deviation and for the two other signals by the  $1\sigma$  confidence interval (error bars might be smaller than the size of the data points).

plication, one is interested in filling the target structure without defects in the shortest possible time. We have therefore performed a second measurement series, with the goal to fill all target traps from the buffer traps as fast as possible. Evaluating the cumulative success rate for a defect-free target array quantifies in which percentage of realizations the target structure has been achieved in one of the first  $n$  rearrangement cycles. For the six-site hexagonal structure, the cumulative success rate is shown in Fig. 4. After eight rearrangement cycles, we achieve a fully filled structure with 86.8(7)% probability, while a cumulative success rate of 91.5(6)% is observed after 15 cycles. Furthermore, Fig. 4 shows the fraction of loaded buffer traps for every rearrangement cycle. As we do not load atoms into the tweezer array directly from the molasses, all buffer and target traps are empty before the first rearrangement cycle. The first filling of the buffer traps gives a filling fraction of 0.596(4), as expected for single-atom preparation via light-assisted collisions for a sufficiently large number of atoms available in the reservoir. For later cycles, the refill probability is influenced by the change in atom number and temperature in the reservoir trap. The atom number is reduced due to generic loss processes occurring in the unperturbed trap [lifetime = 5(1) s] but is dominated by atom extraction during the first two to three rearrangement cycles.

From this observation and the fact that the reservoir fluorescence and the buffer-trap filling fraction in Fig. 4 show a strongly correlated temporal behavior, we deduce that limitations of our current setup arise from the relatively small number of atoms in the reservoir trap and the inability of reloading. From the  $\sim 80$  atoms initially

trapped in the reservoir, we prepare on average 10(2) atoms in the buffer section. If continuous or repeated reloading could be established, this would make a constant filling of 60% of the buffer traps readily available. Further improvement of the overall performance could be achieved by increasing the current transport efficiency of 75.3(9)% between target and buffer traps. Optimizing the experimental conditions should allow for an increase of the transport efficiencies above 98% as reported in Ref. [37].

To summarize, in this letter, we have presented a method for loading individual atoms from an external reservoir into a tweezer array. We achieve this by repeatedly extracting small atom ensembles from a large dipole trap acting as an atom reservoir using a movable laser beam acting as transport tweezers. During transport, we prepare individual atoms from these ensembles by collisional blockade and store them in the dedicated buffer trap section of our tweezer array. Atoms from this buffer section are transported again to deterministically build up a target structure or refill empty target-structure sites. The reservoir and buffer trap technique can be implemented as an experimental addition to large tweezer arrays which are preloaded with individual atoms by other methods to compensate for atom loss or revoke intentional atom removal.

A straightforward extension of this letter is accessible by the implementation of parallelized operation of the functional modules introduced above. Continuous loading of a tweezer array can be achieved by including a method for repeated refilling of the reservoir trap

with cold atoms. Recently, long-distance transport and continuous supply of ultracold atom clouds have been demonstrated in Refs. [45, 46], matching our requirements. We envision establishing MOT operation in a separated part of the vacuum system and continuously transporting cold-atom clouds into the reservoir trap by a cold-atom beam line. With this, the reduction of the buffer-section reloading probability due to a decrease in the number of atoms in the reservoir will be eliminated, and the continuous provision of individual atoms to fill the target structure will be maintained at a high rate. Combining several cold-atom beam lines delivering different atomic or molecular species with reservoir and tweezer traps holding all species will allow for the efficient implementation of multispecies tweezer arrays for various applications.

## ACKNOWLEDGMENTS

We acknowledge financial support by the Federal Ministry of Education and Research (Grant No. 13N15981), by the Deutsche Forschungsgemeinschaft [Grants No. BI 647/6-1 and No. BI 647/6-2, Priority Program SPP 1929 (GiRyd)], and by the Open Access Publishing Fund of Technische Universität Darmstadt. We thank the *labscript* suite [47] community for support in implementing state-of-the-art control software for our experiments.

---

[1] C. S. Adams, J. D. Pritchard, and J. P. Shaffer, Rydberg atom quantum technologies, *J. Phys. B: At. Mol. Opt. Phys.* **53**, 012002 (2019).

[2] A. Browaeys and T. Lahaye, Many-body physics with individually controlled Rydberg atoms, *Nature Phys* **16**, 132 (2020).

[3] L. Henriet, L. Beguin, A. Signoles, T. Lahaye, A. Browaeys, G.-O. Reymond, and C. Jurczak, Quantum computing with neutral atoms, *Quantum* **4**, 327 (2020).

[4] M. Morgado and S. Whitlock, Quantum simulation and computing with Rydberg-interacting qubits, *AVS Quantum Sci.* **3**, 023501 (2021).

[5] A. M. Kaufman and K.-K. Ni, Quantum science with optical tweezer arrays of ultracold atoms and molecules, *Nature Phys* **17**, 1324 (2021).

[6] X.-F. Shi, Quantum logic and entanglement by neutral Rydberg atoms: methods and fidelity, *Quantum Science and Technology* **7**, 023002 (2022).

[7] I. Cong, H. Levine, A. Keesling, D. Bluvstein, S.-T. Wang, and M. D. Lukin, Hardware-Efficient, Fault-Tolerant Quantum Computation with Rydberg Atoms, *Phys. Rev. X* **12**, 021049 (2022).

[8] K. Wintersperger, F. Dommert, T. Ehmer, A. Hoursanov, J. Klepsch, W. Mauerer, G. Reuber, T. Strohm, M. Yin, and S. Luber, Neutral atom quantum computing hardware: Performance and end-user perspective (2023), arXiv:2304.14360.

[9] M. Endres, H. Bernien, A. Keesling, H. Levine, E. R. Anschuetz, A. Krajenbrink, C. Senko, V. Vuletic, M. Greiner, and M. D. Lukin, Atom-by-atom assembly of defect-free one-dimensional cold atom arrays, *Science* **354**, 1024 (2016).

[10] H. Levine, A. Keesling, G. Semeghini, A. Omran, T. T. Wang, S. Ebadi, H. Bernien, M. Greiner, V. Vuletić, H. Pichler, and M. D. Lukin, Parallel Implementation of High-Fidelity Multiqubit Gates with Neutral Atoms, *Phys. Rev. Lett.* **123**, 170503 (2019).

[11] I. S. Madjarov, J. P. Covey, A. L. Shaw, J. Choi, A. Kale, A. Cooper, H. Pichler, V. Schkolnik, J. R. Williams, and M. Endres, High-fidelity entanglement and detection of alkaline-earth Rydberg atoms, *Nature Phys* **16**, 857 (2020).

[12] S. Ma, A. P. Burgers, G. Liu, J. Wilson, B. Zhang, and J. D. Thompson, Universal gate operations on nuclear spin qubits in an optical tweezer array of  $^{171}\text{Yb}$  atoms, *Phys. Rev. X* **12**, 021028 (2022).

[13] R. Dumke, M. Volk, T. Müther, F. B. J. Buchkremer, G. Birk, and W. Ertmer, Micro-optical Realization of Arrays of Selectively Addressable Dipole Traps: A Scalable Configuration for Quantum Computation with Atomic Qubits, *Phys. Rev. Lett.* **89**, 097903 (2002).

[14] D. Barredo, S. de Léséleuc, V. Lienhard, T. Lahaye, and

A. Browaeys, An atom-by-atom assembler of defect-free arbitrary two-dimensional atomic arrays, *Science* **354**, 1021 (2016).

[15] M. O. Brown, T. Thiele, C. Kiehl, T.-W. Hsu, and C. A. Regal, Gray-Molasses Optical-Tweezer Loading: Controlling Collisions for Scaling Atom-Array Assembly, *Phys. Rev. X* **9**, 011057 (2019).

[16] D. Ohl de Mello, D. Schäffner, J. Werkmann, T. Preuschoff, L. Kohfahl, M. Schlosser, and G. Birk, Defect-Free Assembly of 2D Clusters of More Than 100 Single-Atom Quantum Systems, *Phys. Rev. Lett.* **122**, 203601 (2019).

[17] Y. Wang, S. Shevate, T. M. Wintermantel, M. Morgado, G. Lochead, and S. Whitlock, Preparation of hundreds of microscopic atomic ensembles in optical tweezer arrays, *npj Quantum Information* **6**, 1 (2020).

[18] M. Kim, Y. Song, J. Kim, and J. Ahn, Quantum Ising hamiltonian programming in trio, quartet, and sextet qubit systems, *PRX Quantum* **1**, 020323 (2020).

[19] S. Ebadi, T. T. Wang, H. Levine, A. Keesling, G. Semeghini, A. Omran, D. Bluvstein, R. Samajdar, H. Pichler, W. W. Ho, *et al.*, Quantum phases of matter on a 256-atom programmable quantum simulator, *Nature (London)* **595**, 227 (2021).

[20] P. Scholl, M. Schuler, H. J. Williams, A. A. Eberharter, D. Barredo, K.-N. Schymik, V. Lienhard, L.-P. Henry, T. C. Lang, T. Lahaye, *et al.*, Quantum simulation of 2D antiferromagnets with hundreds of Rydberg atoms, *Nature (London)* **595**, 233 (2021).

[21] C. Sheng, J. Hou, X. He, K. Wang, R. Guo, J. Zhuang, B. Mamat, P. Xu, M. Liu, J. Wang, and M. Zhan, Defect-Free Arbitrary-Geometry Assembly of Mixed-Species Atom Arrays, *Phys. Rev. Lett.* **128**, 083202 (2022).

[22] T. Graham, Y. Song, J. Scott, C. Poole, L. Phuttitarn, K. Jooya, P. Eichler, X. Jiang, A. Marra, B. Grinkemeyer, *et al.*, Multi-qubit entanglement and algorithms on a neutral-atom quantum computer, *Nature (London)* **604**, 457 (2022).

[23] K. Barnes, P. Battaglino, B. J. Bloom, K. Cassella, R. Coxe, N. Crisosto, J. P. King, S. S. Kondov, K. Kotru, S. C. Larsen, *et al.*, Assembly and coherent control of a register of nuclear spin qubits, *Nature Communications* **13**, 2779 (2022).

[24] K.-N. Schymik, B. Ximenez, E. Bloch, D. Dreon, A. Signoles, F. Nogrette, D. Barredo, A. Browaeys, and T. Lahaye, In situ equalization of single-atom loading in large-scale optical tweezer arrays, *Phys. Rev. A* **106**, 022611 (2022).

[25] Z. Z. Yan, B. M. Spar, M. L. Prichard, S. Chi, H.-T. Wei, E. Ibarra-García-Padilla, K. R. A. Hazzard, and W. S. Bakr, Two-Dimensional Programmable Tweezer Arrays of Fermions, *Phys. Rev. Lett.* **129**, 123201 (2022).

[26] W. Tian, W. J. Wee, A. Qu, B. J. M. Lim, P. R. Datla, V. P. W. Koh, and H. Loh, Parallel Assembly of Arbitrary Defect-Free Atom Arrays with a Multitweezer Algorithm, *Phys. Rev. Appl.* **19**, 034048 (2023).

[27] D. Barredo, V. Lienhard, S. De Léséleuc, T. Lahaye, and A. Browaeys, Synthetic three-dimensional atomic structures assembled atom by atom, *Nature (London)* **561**, 79 (2018).

[28] A. Kumar, T.-Y. Wu, F. Giraldo, and D. S. Weiss, Sorting ultracold atoms in a three-dimensional optical lattice in a realization of Maxwell's demon, *Nature (London)* **561**, 83 (2018).

[29] M. Schlosser, S. Tichelmann, D. Schäffner, D. Ohl de Mello, M. Hambach, J. Schütz, and G. Birk, Scalable Multilayer Architecture of Assembled Single-Atom Qubit Arrays in a Three-Dimensional Talbot Tweezer Lattice, *Phys. Rev. Lett.* **130**, 180601 (2023).

[30] P. Huft, Y. Song, T. M. Graham, K. Jooya, S. Deshpande, C. Fang, M. Kats, and M. Saffman, Simple, passive design for large optical trap arrays for single atoms, *Phys. Rev. A* **105**, 063111 (2022).

[31] Y. Chew, T. Tomita, T. P. Mahesh, S. Sugawa, S. de Léséleuc, and K. Ohmori, Ultrafast energy exchange between two single Rydberg atoms on a nanosecond timescale, *Nature Photonics* **16**, 724 (2022).

[32] K. McDonnell, L. F. Keary, and J. D. Pritchard, Demonstration of a Quantum Gate Using Electromagnetically Induced Transparency, *Phys. Rev. Lett.* **129**, 200501 (2022).

[33] L.-M. Steinert, P. Osterholz, R. Eberhard, L. Festa, N. Lorenz, Z. Chen, A. Trautmann, and C. Gross, Spatially Tunable Spin Interactions in Neutral Atom Arrays, *Phys. Rev. Lett.* **130**, 243001 (2023).

[34] N. Schlosser, G. Reymond, and P. Grangier, Collisional Blockade in Microscopic Optical Dipole Traps, *Phys. Rev. Lett.* **89**, 023005 (2002).

[35] A. Jenkins, J. W. Lis, A. Senoo, W. F. McGrew, and A. M. Kaufman, Ytterbium Nuclear-Spin Qubits in an Optical Tweezer Array, *Phys. Rev. X* **12**, 021027 (2022).

[36] A. L. Shaw, P. Scholl, R. Finklestein, I. S. Madjarov, B. Grinkemeyer, and M. Endres, Dark-State Enhanced Loading of an Optical Tweezer Array, *Phys. Rev. Lett.* **130**, 193402 (2023).

[37] K.-N. Schymik, V. Lienhard, D. Barredo, P. Scholl, H. Williams, A. Browaeys, and T. Lahaye, Enhanced atom-by-atom assembly of arbitrary tweezer arrays, *Phys. Rev. A* **102**, 063107 (2020).

[38] C. Sheng, J. Hou, X. He, P. Xu, K. Wang, J. Zhuang, X. Li, M. Liu, J. Wang, and M. Zhan, Efficient preparation of two-dimensional defect-free atom arrays with near-fewest sorting-atom moves, *Phys. Rev. Res.* **3**, 023008 (2021).

[39] B. Cimring, R. E. Sabeh, M. Bacvanski, S. Maaz, I. E. Hajj, N. Nishimura, A. E. Mouawad, and A. Cooper, Efficient algorithms to solve atom reconfiguration problems. I. The redistribution-reconfiguration (red-rec) algorithm (2022), arXiv:2212.03885.

[40] R. E. Sabeh, J. Bohm, Z. Ding, S. Maaz, N. Nishimura, I. E. Hajj, A. E. Mouawad, and A. Cooper, Efficient algorithms to solve atom reconfiguration problems. II. The assignment-rerouting-ordering (aro) algorithm (2022), arXiv:2212.05586.

[41] K. Singh, S. Anand, A. Pocklington, J. T. Kemp, and H. Bernien, Dual-Element, Two-Dimensional Atom Array with Continuous-Mode Operation, *Phys. Rev. X* **12**, 011040 (2022).

[42] M. Schlosser, J. Kruse, C. Gierl, S. Teichmann, S. Tichelmann, and G. Birk, Fast transport, atom sample splitting and single-atom qubit supply in two-dimensional arrays of optical microtraps, *New J. Phys.* **14**, 123034 (2012).

[43] D. Schäffner, T. Preuschoff, S. Ristok, L. Brozio, M. Schlosser, H. Giessen, and G. Birk, Arrays of individually controllable optical tweezers based on 3D-printed microlens arrays, *Opt. Express* **28**, 8640 (2020).

[44] S. J. M. Kuppens, K. L. Corwin, K. W. Miller, T. E.

Chupp, and C. E. Wieman, Loading an optical dipole trap, *Phys. Rev. A* **62**, 013406 (2000).

[45] T. Klostermann, C. R. Cabrera, H. von Raven, J. F. Wienand, C. Schweizer, I. Bloch, and M. Aidelsburger, Fast long-distance transport of cold cesium atoms, *Phys. Rev. A* **105**, 043319 (2022).

[46] C.-C. Chen, R. González Escudero, J. Minář, B. Pasquiou, S. Bennetts, and F. Schreck, Continuous Bose–Einstein condensation, *Nature (London)* **606**, 683 (2022).

[47] P. Starkey, C. Billington, S. Johnstone, M. Jasperse, K. Helmerson, L. Turner, and R. Anderson, A scripted control system for autonomous hardware-timed experiments, *Rev. Sci. Instrum.* **84**, 085111 (2013).